The use of chemometrics to study multifunctional indole alkaloids from Psychotria nemorosa (Palicourea comb. nov.) : part II: indication of peaks related to the inhibition of butyrylcholinesterase and monoamine oxidase-A

The use of chemometrics to study multifunctional indole alkaloids from *Psychotria nemorosa* (*Palicourea comb. nov.*). Part II: indication of peaks related to the inhibition of butyrylcholinesterase and monoamine oxidase-A

Luiz C. Klein-Júnior[a,b], Johan Viaene[a], Emmy Tuenter[c], Juliana Salton[b], André L. Gasper[d], Sandra Apers[c], Jan P.M. Andries[e], Luc Pieters[c], Amélia T. Henriques[b], Yvan Vander Heyden[a,*]

[a] Department of Analytical Chemistry and Pharmaceutical Technology, Center for Pharmaceutical Research (CePhaR), Vrije Universiteit Brussel – VUB, Laarbeeklaan 103, B-1090 Brussels, Belgium

[b] Laboratory of Pharmacognosy and Quality Control of Phytomedicines, Faculty of Pharmacy, Universidade Federal do Rio Grande do Sul - UFRGS, Av. Ipiranga 2752, 90610-000, Porto Alegre/RS, Brazil

[c] Natural Products & Food Research and Analysis, Department of Pharmaceutical Sciences, University of Antwerp, Universiteitsplein 1, B-2610 Antwerp, Belgium

[d] Herbarium Dr. Roberto Miguel Klein, Department of Natural Sciences, Universidade Regional de Blumenau - FURB, R. Antonio da Veiga 140, 89012-900, Blumenau/SC, Brazil

[e] Research Group Analysis Techniques in the Life Sciences, Avans Hogeschool, University of Professional Education, P.O. Box 90116, 4800 RA Breda, The Netherlands

[*] Corresponding author. Tel.: +32 2 477 47 34, fax: +32 2 477 47 35. E-mail addresses: yvanvdh@vub.ac.be, Yvan.Vander.Heyden@vub.ac.be (Y. Vander Heyden).

ABSTRACT

Psychotria nemorosa is chemically characterized by indole alkaloids and displays significant inhibitory activity on butyrylcholinesterase (BChE) and monoamine oxidase-A (MAO-A), both enzymes related to neurodegenerative disorders. In the present study, 43 samples of *P. nemorosa* leaves were extracted and fractionated in accordance to previously optimized methods (see Part I). These fractions were analyzed by means of UPLC-DAD and assayed for their BChE and MAO-A inhibitory potencies. The chromatographic fingerprint data was first aligned using correlation optimized warping and Principal Component Analysis to explore the data structure was performed. Multivariate calibration techniques, namely Partial Least Squares (PLS1), PLS2 and Orthogonal Projections to Latent Structure (O-PLS1), were evaluated for modelling the activities as a function of the fingerprints. Since the best results were obtained with O-PLS1 model (RMSECV = 9.3 and 3.3 for BChE and MAO-A, respectively), the regression coefficients of the model were analyzed and plotted relative to the original fingerprints. Four peaks were indicated as multifunctional compounds, with the capacity to impair both BChE and MAO-A activities. In order to confirm these results, a semi-prep HPLC technique was used and a fraction containing the four peaks was purified and evaluated *in vitro*. It was observed that the fraction exhibited an IC_{50} of 2.12 μg mL^{-1} for BChE and 1.07 μg mL^{-1} for MAO-A. These results reinforce the prediction obtained by O-PLS1 modelling.

Keywords: chromatographic fingerprinting; multivariate calibration technique; indole alkaloid; neurodegenerative disorders; multifunctional compounds.

1. Introduction

Plants are known as impressive chemical factories and have been playing an important role in drug discovery. Nevertheless, pharmaceutical companies have reduced the economic input in this research field, mainly because of difficulties related to the re-isolation of known metabolites and the lack of reliable tools for the indication of active compounds [1]. However, several new strategies and technologies are nowadays available and have been successfully applied for the identification of leads in natural products research [1-5]. One of these strategies is the metabolic profiling approach. It correlates the chemical profile and the biological activity of extracts or fractions, guiding the isolation and early identification of the targeted secondary metabolites [2,6-10].

Different plants have been studied by this metabolic profiling strategy, focusing on a wide variety of secondary metabolites, such as terpenoids [11], flavonoids [2], and alkaloids [12]. Alkaloids make up around 20% of the natural substances described so far, and have a structural diversity that is comparable to terpenoids. These nitrogenous compounds usually are pharmacologically active, being the main group of secondary metabolites of interest to researchers and the pharmaceutical industry. These metabolites are predominantly found in angiosperms, mainly in Apocynaceae, Solanaceae, Papaveraceae, Loganiaceae, and Rubiaceae [13,14].

Alkaloids are widely known for their potential to treat central nervous system (CNS) related diseases. Several bioactive alkaloid-like structures are reported in the literature, however probably the best known examples are the indole alkaloids derivatives, as rivastigmine and galantamine, used for the treatment of Alzheimer's disease [15]. In addition, some of these compounds have been investigated because of their multifunctional activities, also related to

other targets in neurodegenerative processes, such as the inhibition of monoamine oxidases (MAO) [16].

The plants belonging to the genus *Psychotria* L. (Rubiaceae) are widely used because of the different effects they can promote in the CNS. Amazon Indian tribes use these plants for the preparation of Ayahuasca, a hallucinogenic beverage for medicinal, ritual and recreational purposes [17]. In the traditional medicine of Middle America, *Psychotria* species are used for the treatment of dementia related effects [18]. In fact, our research group has also demonstrated the modulatory action of *Psychotria* alkaloid fractions and isolated compounds on enzymes related to neurodegenerative disorders, such as acetylcholinesterase (AChE), butyrylcholinesterase (BChE), MAO-A, sirtuins, and catechol-*O*-methyltransferase (COMT) [16,19-22]. It is worthwhile to mention that several *Psychotria* subg. *Heteropsychotria* species have been transferred to the *Palicourea* genus, based on taxonomic and chemical aspects [23,24]. Taking this into account, *Palicourea comb. nov.* was added to the original *Psychotria* subg. *Heteropsychotria* names, in accordance with this trend [23,24].

Recently, we demonstrated that the alkaloid fraction obtained from *Psychotria nemorosa* Gardner (*Palicourea comb. nov.*), was able to significantly inhibit MAO-A and BChE activities [25]. In addition, the species exhibited a high chemical diversity. In order to access the alkaloid metabolite profile, optimized extraction and fractionation methods were developed in the first part of this study [26]. In the actual paper, this optimized extraction procedure was applied to several samples of *P. nemorosa* and the alkaloid fractions were analyzed by means of UPLC-DAD. All fractions were evaluated *in vitro* for their MAO-A and BChE inhibitory activities and these results were modelled by different multivariate calibration techniques as a function of their chromatographic fingerprints, aiming the indication of peaks potentially responsible for the pharmacological activities.

2. Material and methods

2.1 Chemicals

Kynuramine dihydrobromide, clorgyline hydrochloride, pargyline hydrochloride, tacrine, galanthamine, 5,5′-dithiobis-(2-nitrobenzoic acid), acetylthiocholine iodide, electric eel acetylcholinesterase, *S*-butyrylthiocholine iodide, horse serum butyrylcholinesterase, and DMSO were purchased from Sigma Chemical Co. (St. Louis, MO, USA). Human MAO-A and MAO-B SupersomesTM were acquired from BD Gentest (Woburn, MA, USA). UPLC-MS grade solvents were acquired from Actu-All Chemicals (Oss, The Netherlands). All remaining solvents were acquired from Tedia Company (Fairfield, CA, USA).

2.2 Plant material

The leaves of *P. nemorosa* were collected from forty three individuals distributed in five different places of Blumenau/SC, Brazil (Fig. 1). Vouchers of each collection were deposited in the Dr. Roberto Miguel Klein Herbarium under the numbers FURB 43759, 43756, 43758, 43755, 43580. The identification of the species was performed by the botanic André L Gasper (FURB/Brazil). Access authorization was given by CNPq/Brazil under the number 010772/2014-6. The vegetal material was dried in an air oven at 40 °C for 48h (Lawes, Brazil), ground using an analytical mill (IKA, Königswinter, Germany), and sieved (≤180 μm) using a mechanical shaker Retac 3D (RETSCH, Haan, Germany).

126 *2.3 Extraction and fractionation procedures*

127

128 The optimized extraction and fractionation methods were previously described [26].
129 Briefly, vegetal material was submitted to ultrasound assisted extraction using an ultrasonic bath
130 (132 W; 40 kHz) during 65 min at 45 °C. Methanol was used as extraction solvent at a 1:50
131 (m/v) drug:solvent ratio. Vegetal material particle size was ≤ 180 µm. The extracts were filtered
132 and then evaporated at 40 °C using a rotary evaporator with a vacuum pump (V-710, Büchi,
133 Flawil, Switzerland). Before fractionation experiments, the samples were kept for two weeks
134 under vacuum in a desiccator containing activated silica gel beads.

135 For fractionation, a solid phase extraction method was developed applying a Box-
136 Behnken design [26]. Briefly, normal-phase silica cartriges (Supelclean LC-Si, Supelco, PA,
137 USA) were equilibrated with 10 mL of HCl 1M. Before dryness, the samples (150 mg mL^{-1} in HCl
138 1M) were loaded and the cartridges dried. Then, the cartridges were washed using 10 mL of
139 dichloromethane. After dryness, the samples were eluted with 30 mL of 5% NH_4OH in
140 dichloromethane/acetonitrile (6:4, v/v) (gravity flow). The resulting organic extracts were
141 concentrated to dryness by a tube evaporator at 40 °C, resulting in the fractions enriched in
142 alkaloids. These samples were kept for one week under vacuum in a desiccator containing
143 activated silica gel beads.

144

145 *2.4 Fingerprint Development*

146

147 A system composed by an ACQUITY I-class UPLC® from Waters (Milford, MA, USA)
148 was used. The separation was performed on a 50 mm × 2.1 mm i.d., 1.7 µm, Acquity BEH C_{18}
149 UPLC column (Waters) at 40 °C and a flow rate of 0.3 mL min^{-1} with a mobile phase consisting
150 of water (formic acid 0.1%) (A) and methanol (B) in the following gradient: 0 min (99 (A): 1 (B),
151 v/v), 1 min (94:6), 4 min (94:6), 24 min (54:46), 25 min (54:46), 26 min (48:52), 28 min (48:52),

29 min (0:100), 33 min (0:100), 35 min (99:1), 40 min (99:1). A 2 µl aliquot of the samples was injected twice and the detection was performed at 280 nm. The solutions were freshly prepared in methanol before each experiment and filtered through a 0.22 µm cellulose regenerated membrane filter. Data was processed using Waters MassLynx software.

2.5 Enzymatic assays

2.5.1 Cholinesterases inhibitory assays

First, all fractions were assayed both for AChE and BChE at 100 µg mL^{-1}. For the AChE inhibitory assay, wells were filled with 158 µL Ellman's reagent (0.15 mM 5,5′-dithiobis-(2-nitrobenzoic acid) in 0.1 M phosphate buffer pH 7.4), 20 µL acetylthiocholine iodide solution (0.33 mM), and 2 µL test compound solution in DMSO. The addition of 20 µL electric eel AChE solution (1 U.I. mL^{-1} in 0.1 M phosphate buffer pH 7.4, containing human serum albumin at 1 mg mL^{-1}) started the reaction and the absorbance at 412 nm was monitored for 6 min (intervals of 40 seconds between readings) in a microplate reader (SpectraMax, Molecular Devices, CA, USA). For the BChE assay, S-butyrylthiocholine iodide was used as substrate and horse serum BChE (1 U.I. mL^{-1} in 0.1 M phosphate buffer pH 7.4, containing human serum albumin at 1 mg mL^{-1}) was used to start the reaction. The same measurement procedure as above was used. The linearity of the increase in absorbance as a function of time was checked for each sample and the difference between the final and starting readings was calculated and compared to the negative control (DMSO). Galanthamine and tacrine were used as positive controls.

Taking into account that only BChE was significantly inhibited at 100 µg mL^{-1} (≥ 50% inhibition), in a second step the IC_{50} was calculated for each sample using concentrations ranging from 0.5 to 200 µg mL^{-1} (quadruplicate). For the semi-purified fraction, concentrations ranged from 0.25 to 100 µg mL^{-1}.

178 *2.5.2 Monoamine oxidase inhibitory assays*

179 All fractions were assayed at 100 µg mL^{-1} for MAO-A and MAO-B activities. Human
180 recombinant MAO-A or MAO-B were used for the assays. Black polystyrene 96-well microtiter
181 plates were preincubated for 20 min at 37 °C containing 158 µL potassium phosphate buffer pH
182 7.4, 2 µL sample diluted in DMSO and 20 µL kynuramine 0.5 mM (substrate). Later, 20 µL
183 enzyme (MAO-A 0.09 mg mL^{-1} or MAO-B 0.15 mg mL^{-1}) was added, followed by an incubation
184 period (30 min at 37°C). Finally, 75 µL of NaOH 2M was used to stop the reaction.
185 Fluorescence readings were made on a Wallac EnVision high throughput screening microplate
186 reader (PerkinElmer Life and Analytical Sciences, Turku, Finland), at an excitation wavelength
187 of 315 nm and an emission wavelength of 380 nm. As negative control, DMSO was used.
188 Clorgyline (MAO-A inhibition) and pargyline (MAO-B inhibition) were used to monitor the
189 experiment as positive controls. Since only MAO-A was significantly inhibited at 100 µg mL^{-1} (≥
190 50% inhibition), in a second step the IC_{50} was calculated for each sample using concentrations
191 ranging from 0.5 to 200 µg mL^{-1} (triplicate). For the semi-purified fraction, concentrations ranged
192 from 0.25 to 100 µg mL^{-1}.
193
194 *2.6 Data analysis*
195
196 All fingerprint data analysis was performed using Matlab 2013b (The Mathworks, Natick,
197 MA). Data (pre)processing was performed using m-files written for Matlab. The IC_{50} were
198 calculated by modelling the experimental data (curves representing % of inhibition versus
199 concentration) building a quadratic regression model with Prism 5.0 (GraphPad Software, CA,
200 USA).
201
202
203

204 *2.6.1 Data preprocessing*

205 The data matrix **X** consisted of the samples (rows; *n*=43) and the time points (columns; *p*
206 = 36001). Each element of the matrix contained the detection signal (intensity) for a given
207 sample at a given time point. Prior to data analysis, different preprocessing techniques were
208 used to have equivalent information for the chromatographic profiles. In a first step, correlation
209 optimized warping (COW) was applied as a peak alignment technique in order to correct small
210 shifts which occur due to small variations in mobile phase composition, instrument instability,
211 and column ageing. It aligns the chromatograms by linear stretching and compression of
212 segments of the fingerprint data in order to improve the correlation between the chromatogram
213 to be aligned (*P*) and the targeted chromatogram (*T*). Each section is aligned accordingly to the
214 shift of the section's end point by a maximal limit defined as the slack parameter *t*. Applying –*t* to
215 *t*, the correlation coefficients are calculated for all possibilities. The warped section which best
216 correlates to the corresponding section of *T* is maintained and the aligned fingerprint is built by
217 the combination of all optimally aligned sections [27].

218 Taking into account that useful information is given by the variation of the variables
219 between samples, and not by the absolute values, additional preprocessing approaches can be
220 applied in order to remove interferences in the analysis. In this study, three approaches were
221 evaluated: column centering (removes the column mean from each corresponding value);
222 normalization (scales the columns to a constant total); and the standard normal variate (SNV)
223 transformation (scales the rows to a constant total) [7].

224

225 *2.6.2 Exploratory analysis – Principal Component Analysis*

226 Principal Component Analysis (PCA) is used to explore or visualize the data structure in
227 a matrix **X**, reducing the *p* variables to a limited number of informative latent variables, the
228 Principal Components (PCs). The first PCs (PC1, PC2,…) retain most of the information from
229 the entire data. The PCs are orthogonal to each other and they maximize the description of the

variance in the matrix **X**. The projection of the *n* objects from the original data space on a PC represents the scores. The loadings are given by the contribution of the original variables to the score on a PC [28].

2.6.3 Linear multivariate calibration techniques

Linear multivariate calibration techniques correlate the data in a matrix **X** (*n* x *p*) (here the fingerprints) to an *n* x 1 response vector **y** (here the inhibitory activities). This relationship can be described as:

$$\boldsymbol{y} = \boldsymbol{Xb} + \boldsymbol{e} \quad (1)$$

where **b** represents a *p* x 1 vector of regression coefficients and **e** an *n* x 1 residual vector.[7] Two linear multivariate calibration techniques were used in this study: Partial Least Squares (PLS) and Orthogonal Projections to Latent Structures (O-PLS1). The regression coefficients were evaluated to indicate the peaks that might be responsible for the BChE and MAO-A inhibitory activities [7].

2.6.3.1 Partial Least Squares (PLS1)

Partial Least Squares (PLS1) is a latent-variable regression technique which expresses the relationship between **X** and **y**. The model can be written as follows:

$$\boldsymbol{X} = \boldsymbol{TP^T} + \boldsymbol{E} \quad (2)$$

$$\boldsymbol{y} = \boldsymbol{TP^T b} + \boldsymbol{f} = \boldsymbol{Tq} + \boldsymbol{f} \quad (3)$$

$$\boldsymbol{b} = \boldsymbol{Pq} \quad (4)$$

where **T** represents the *n* x *n* score matrix for **X** and **y**, **P** the *p* x *n* loading matrix of **X** on **T** and $\mathbf{P}^T$ its transposal, **E** the *n* x *p* residual matrix of **X**, **b** the *p* x 1 vector of regression coefficients, **q** the *n* x 1 loading vector of **y** on **T**, and **f** the *n* x 1 residual vector of **y** [6]. The optimal model complexity was determined by leave-one-out cross-validation procedure (LOO-CV). The root mean squared error of cross-validation (RMSECV) was calculated for each model:

$$\boldsymbol{RMSECV} = \sqrt{\sum_{\boldsymbol{i}=\boldsymbol{1}}^{\boldsymbol{N}} \frac{(\hat{y}_{\boldsymbol{cv},\boldsymbol{i}} - \boldsymbol{y_i})^{\boldsymbol{2}}}{\boldsymbol{N}}} \quad (5)$$

where **N** the number of calibration samples, $\boldsymbol{y_i}$ the measured response for the *i*th sample, and $\hat{y}_{\boldsymbol{cv},\boldsymbol{i}}$ the corresponding response predicted by the calibration model built without the *i*th sample [7].

2.6.3.2 Partial Least Squares with Several Responses (PLS2)

As an alternative to building individual models for each response (BChE and MAO-A inhibitory activities), PLS2 is able to provide one model for several responses, allowing also a simultaneous graphical inspection. The matrix of PLS2 regression coefficients, **B** (*K* x *M*), can be calculated as:

$$\boldsymbol{B} = \boldsymbol{W}\left(\boldsymbol{P}^{\boldsymbol{T}}\boldsymbol{W}\right)^{-\boldsymbol{1}}\boldsymbol{Q} \quad (6)$$

where **W** (*K* x *A*) is the X weight matrix, **P** (*K* x *A*) the X-loading matrix, and **Q** (*M* x *A*) the Y-loading matrix. *K* is the number of predictor variables in the **X** (*N* x *K*) matrix, *M* the number of

responses in the **Y** (*N* x *M*) matrix, *A* the number of PLS2 factors, and *N* the number of objects [29].

The predictive ability of PLS2 model was evaluated by internal validation, resulting in the RMSECV:

$$\boldsymbol{RMSECV} = \sqrt{\frac{1}{N_{cal}M}\sum_{i=1}^{N_{cal}}\sum_{j=1}^{M}\left(\boldsymbol{y_{ij}} - \boldsymbol{\hat{y}_{ij}}\right)^2} \quad (7)$$

where y_{ij} and $\hat{y}_{ij}$ are the experimental and predicted responses, respectively for the left—out elements from the training set during cross validation, N_{cal} the number of calibration samples in the training set, and *M* the number of responses [29].

2.6.3.3 Orthogonal Projections to Latent Structures (O-PLS1)

Orthogonal Projections to Latent Structures (O-PLS1) is a modification of PLS1, which removes the variation in the original matrix data that is not correlated to *y*. In this case, the original data is split into two data sets: one that contains the *y*-relevant information and one with the orthogonal data. The model can be written as follows:

$$\boldsymbol{X} = \boldsymbol{TP^T} + \boldsymbol{T_{orth}P_{orth}^T} + \boldsymbol{E} \quad (8)$$

where **T** represents the orthonormal *n* x *n* score matrix for **X** and **y**, **P** the orthonormal *p* x *n* loading matrix corresponding to the regression coefficients of **X** on **T** and $\mathbf{P}^{\mathsf{T}}$ its transposal, $\boldsymbol{T_{orth}}$ the orthogonal *n* x *n* score matrix for **X** and **y**, $\boldsymbol{P_{orth}}$ represents the orthogonal *p* x *n* loading matrix and $\boldsymbol{P_{orth}^T}$ its transposal, and **E** the *n* x *p* residual matrix of **X** [7].

By removing the orthogonal information from the original **X** matrix, the complexity of the model can be reduced to a single factor, which facilitates the interpretability of the regression coefficients [30].

2.7 Purification procedures

2.7.1 Semi-preparative HPLC purification

A pool of the samples was submitted to the extraction and fractionation procedures, briefly described earlier. This alkaloid fraction was further used for purification by semi-preparative HPLC-DAD. Experiments were performed in a system composed of a HPLC Model 2695 Waters Alliance analytical module equipped with a 2998 photodiode array detector, and a computerized data station equipped with Waters Empower software. A C_{18} Waters XBridge™ (250 mm x 10 mm, 5 µm) column was eluted at a 1.6 mL min^{-1} flow rate with a mobile phase consisting of water (formic acid 0.1%) (A) and methanol (B) in the following gradient: 0 min (85 (A): 15 (B) v/v), 7 min (60:40), 12 min (50:50), 20 min (0:100), 30 min (0:100). Each time, 80 µL of a sample at 50 mg mL^{-1} was injected. The detection was performed at 280 nm. The fraction collected between 5 and 15 min was evaporated using a rotary evaporator and the water removed by lyophilization (Micromodulyo, Savant, MI, USA). This fraction was analyzed by means of UPLC-QToF and fLC-SPE-NMR.

2.7.1.1 UPLC-QToF

Samples were analyzed by a UPLC-QToF system (Waters). UPLC conditions were previously described in section 2.4. MS analyses were performed on a Xevo-G2S-QToF equipment (Waters), in a m/z 50–1200 Da range, with a capillary voltage of 3000V, a cone voltage of 40V, a source temperature at 120°C, and a desolvation temperature at 450°C. The

desolvation gas (97% nitrogen) was obtained through a nitrogen generator (Parker, Nivelles, Belgium) and was kept at a flow of 800 L h^{-1}. Data was recorded in centroid and it was processed using MassLynx V 4.1 software (Waters).

2.7.1.2 LC-SPE-NMR

In order to obtain information about the compounds present in this fraction, it was submitted to LC-SPE-NMR. An Agilent 1200 series HPLC with degasser, quaternary pump, automatic injection and DAD detector, connected to a Bruker/Spark solid phase extraction system using 2 mm Hyspher resin GP (polydivinyl-benzene) cartridges to collect the compounds was used. A Zorbax RX-C18 (Agilent Technologies), 25 cm x 4.6 mm, 5 µm) column was applied at a mobile-phase flow rate of 0.7 mL min^{-1} and a gradient elution was performed with water (trifluoroacetic acid 0.1%) (A) and methanol (B) in the following gradient: 0-24 min (90 (A): 10 (B) v/v), 25 min (80:20), 40 min (70:30), 50-55 min (0:100). A Gilson Liquid Handler 215 was used for preparing the samples for NMR. The detection was performed at 210, 280 and 300 nm. 25 µL of the sample at 10 mg mL^{-1} was injected repetitively and the peaks of interest were collected using the multitrapping function during 3x7 runs. Loaded SPE cartridges were dried with nitrogen gas and the adsorbed compounds eluted using CD_3OD (99.8% D, Aldrich) into 3 mm NMR tubes.

NMR spectra were recorded on a Bruker DRX 400 MHz instrument operating at 400 MHz, employing a 3 mm inverse broadband (BBI) probe using a pulse sequence based on the 1D version of the NOESY sequence, with double solvent presaturation suppressing any residual water and methanol signals (pulse program 'lc1pnf2'). 32 K data points were recorded with a sweep width of 8013 Hz and an acquisition time of 2.04 s. Topspin version 1.3 was used to process the data and a line broadening of 1 Hz was applied.

3. Results and discussion

3.1 Enzymatic inhibitory activities

Recently our research group demonstrated the MAO-A and BChE inhibitory activities of the alkaloid fraction of *P. nemorosa* leaves [25]. In the present study, forty three samples of the same species were collected in different places. The alkaloid fractions obtained by optimized and standardized extraction and fractionation methods were evaluated for their inhibitory effect on MAOs and ChEs activities. First, all samples were evaluated for all MAOs and ChEs isoforms at 100 μg mL^{-1}. However, none of the alkaloid fractions was able to impair MAO-B and AChE activities in an extent higher than 50%. This is usually used as cutoff value, since it means that the IC_{50} should be higher than 100 μg mL^{-1}, demonstrating low interaction with these enzymes and cannot be considered promising [19,20]. Thus, further experiments were only carried on with MAO-A and BChE enzymes.

For IC_{50} determination, fractions were evaluated in concentrations between 0.5 and 200 μg mL^{-1}. For BChE, the IC_{50} ranged from 2.8 to 74 μg mL^{-1}. BChE is mainly expressed in glial cells. However, the enzyme is also present in some neurons in the hippocampus, amygdala and thalamus. Although traditionally BChE is not associated with neurodegeneration and, in fact, with any function, studies in the last decade have been demonstrating that this enzyme actually plays an important role in neurotransmission [31]. Some *in vivo* evidences demonstrate that a specific BChE inhibition resulted in a significant increase of acetylcholine levels [32]. In addition, in *ACHE* knockout mice, BChE was able to compensate AChE absence [33]. In neurodegenerative disorders, such as Alzheimer's and Parkinson's disease, it has been observed that levels of AChE and acetylcholine are reduced, while BChE levels increase, once again indicating that BChE can substitute AChE activity [34,35]. In fact, the inhibition of BChE

can be used as a strategy for the treatment of dementia associated to Alzheimer's and Parkinson's disease [31].

Regarding MAO-A activity, the IC_{50} varied from 1.0 to 18.3 μg mL^{-1}. MAO-A is an enzyme related to the degradation of monoamines, as serotonin, norepinephrine and dopamine. Inhibitors of MAO-A have been traditionally used for the treatment of depression. However, some evidences have been demonstrating that MAO-A expression is higher in patients with Alzheimer's disease [36]. In addition, it has been demonstrated that MAO-A plays an important role in the induction and regulation of apoptosis of neurons during neurodegeneration [37-39]. These findings support the use of MAO-A inhibitors for the treatment of neurodegenerative disorders. Both MAOs and ChEs have been proposed as important targets for multi-target compounds aiming the treatment of neurodegenerative disorders [16,40].

3.2 UPLC fingerprints and pharmacological activities correlation

UPLC fingerprints have been previously developed [26]. As visualized in Figure 2, fingerprints were very similar, with limited qualitative and quantitative variation. This was expected, since samples were collected in the same city and during the same period of the year. Even so, some pharmacological variation was observed, mainly for the BChE activity, which may correlate to some minor chemical changes which are not easily visualized.

In the next sections, chromatographic fingerprints will be linked to the MAO-A and BChE inhibitory activities by linear multivariate calibration techniques. Through the analysis of the regression coefficients of the calibration model, peaks that might be related to the activity will be indicated. Prior to model construction, the fingerprint data is aligned and evaluated by exploratory analysis.

404 *3.2.1 Alignment procedure*

405 As observed in Figure 2a, some shifts in the retention times occurred between the
406 fingerprints, demonstrating the need for alignment of the corresponding peaks. In this study,
407 COW was used. Taking into account the available DAD data and an exploratory analysis, the
408 chromatograms were stretched and compressed to match as good as possible chromatogram
409 79 (second injection of sample 39), which was selected as target chromatogram, since it had
410 the highest mean correlation coefficient with the other chromatograms. The warping results can
411 be observed in Figure 2b. The correlation improvement is clear, both from the warped
412 chromatograms and at the color maps. In addition, correlation to the target chromatogram
413 ranged from 0.44 to 0.98 prior to warping, and between 0.77 and 0.98 after alignment.
414
415 *3.2.2 Exploratory analysis – Principal Component Analysis*

416 To verify whether groups of samples could be distinguished, occasionally according to
417 their pharmacological activity, Principal Component Analysis (PCA) was applied. When
418 examining the PC1-PC2 score plot (data not shown), no cluster formation was observed. In
419 fact, no correlation was seen neither to BChE nor to MAO-A inhibitory activity. Especially in the
420 former case, a small variation in the activity (IC_{50}) was demonstrated (1-18 μg mL^{-1}), which may
421 hamper dense cluster formation.
422
423 *3.2.3 Multivariate calibration techniques*

424 Multivariate calibration models were built for both activities (BChE and MAO-A inhibition)
425 using two techniques: PLS (PLS1 and PLS2) and O-PLS1. Matrix **X** consisted of 43 fingerprints
426 with each 36001 time points, and the IC_{50} of both enzymatic assays were used individually as
427 response vector **y**. Since the final goal of the study was not the prediction of the enzymatic
428 inhibitory activities of new samples, and because of the rather small data set, it was not divided
429 into calibration and validation sets. For model optimization, evaluating the predictive capacity of

the enzymatic inhibitory activity, the leave-one-out cross validation procedure was used prior to the analysis of the regression coefficients to indicate the peaks that might be responsible for the activities. These peaks are indicated as negative peaks in the regression coefficients plot, because of lower IC_{50} means a higher activity.

3.2.3.1 Butyrylcholinesterase inhibition

Using different pretreatment strategies for both PLS1 and O-PLS1 modelling, the best results were obtained by standard normal variate (SNV) followed by column centering, resulting in RMSECV of 10.2 and 9.3, respectively, for 7 PLS-factors. As already mentioned earlier, O-PLS1 modelling usually gives better results, since it removes the variation in **X** that do not correlates to **y** [7,8]. This improvement was also observed in the regression coefficients of the models (Fig. 3 a). Those from PLS1 modelling are very noisy, making the regression coefficients plot interpretation and indication of potentially active peaks difficult. On the other hand, from O-PLS1 modelling, an improvement in the interpretability of the regression coefficients is seen (Fig. 3a).

The major negative coefficient peaks, corresponding to the compounds that might inhibit BChE activity mainly are concentrated at the beginning of the elution, between 1 and 10 min. In addition, some peaks close to 20 min might also be pharmacologically active. Compared to the chromatograms, a match between the negative coefficient peaks and compound peaks is detected, indicating that these compounds may have the capacity to interact to the BChE active site and to impair its activity.

3.2.3.2 Monoamine oxidase-A inhibition

Applying the procedure described for BChE inhibitory peaks, both PLS1 and O-PLS1 models were built for regression coefficients analysis. Using different pretreatment methods, the most suitable for the MAO-A data was column centering, resulting in models with a RMSECV of

456 3.37 for PLS1 (4 PLS-factors) and 3.26 for O-PLS1. Despite the very similar results for
457 RMSECV, again the regression coefficients plots from O-PLS1 were much less noisy (Fig. 3b).
458 As observed for the BChE results, the major negative peaks were again concentrated at the
459 beginning of the regression coefficients plots, corresponding to peaks eluting between 1-10 min
460 in the chromatographic fingerprint.
461
462 3.2.3.3 Multifunctional approach
463 Since the major aim of this study was to identify compounds that might have a
464 multifunctional activity, both on BChE and on MAO-A, the use of PLS2 was evaluated. The best
465 results were obtained for 6 latent variables. However, as observed for PLS1, regression
466 coefficients were very noisy (Fig. 4), impairing its interpretation. As an alternative, both
467 regression coefficient plots obtained by O-PLS1 modelling of the chromatographic fingerprints
468 were compared to the original chemical profile. As observed in Figure 5, it is possible to indicate
469 4 main peaks that seem to play a role for both activities, with retention times of: 1.45, 2.45, 4.15
470 and 9.30 min (1-4, respectively).
471 Since all potentially active peaks eluted between 1 and 10 min, a pool of all samples was
472 prepared and its alkaloid fraction was submitted to fractionation by semi-prep HPLC. The first
473 fraction, corresponding to $1/3^{th}$ of the UPLC chromatogram, i.e. containing all potentially active
474 peaks, was collected and evaluated for its inhibitory effect. The fraction was also injected at the
475 UPLC-DAD in order to check if important peaks (1-4) were present. Based on retention times
476 and UV profiles, it is possible to infer that the peaks indicated in Figure 5 are the same as those
477 collected by semi-prep HPLC and indicated in Figure 6. Varying the concentration from 0.25 to
478 100 µg mL^{-1}, it was observed that the fraction exhibited an IC_{50} of 2.12 µg mL^{-1} for BChE and
479 1.07 µg mL^{-1} for MAO-A. These results highly confirm that the most active compounds are
480 present in this fraction, reinforcing that O-PLS1 modelling coefficients are indicating active
481 multifunctional compounds.

UV spectral data of the multifunctional peaks suggested the presence of indole alkaloids, already expected taking into account previous research of the genus [16,19,25]. MS analysis demonstrated that peaks 1-3 seem to be regular small indole alkaloids ($[M+H]^+$ at 203), such as carbolines and/or tryptamines. However, for peak 4, the presence of a monoterpene indole alkaloid with a glucose moiety ($[M+H]^+$ at 561.2503]) is suggested, as already reported for *Psychotria* species [16,19,20]. Peaks purities were ≥99%.

LC-SPE-NMR analysis resulted in the collection of the 4 potentially active peaks from this fraction, confirmed by UV and MS data. The ^{1}H-spectrum of one of them showed a pattern typical for a 1,3,4-substituted aromatic ring (δ 7.19, d, J = 8.8 Hz, 1H; 6.86, d, J = 2.1 Hz, 1H; 6.75, dd, J = 8.6, 2.2 Hz, 1H), such as a substituted indol- or isoquinoline ring. The ^{1}H-NMR spectra of two other compounds showed two doublets in the aromatic region with J = 8.5 – 8.7 Hz., indicative for two protons in *ortho*-position of each other (δ 7.22, d, J = 8.5 Hz, 1H; 6.76, d, J = 8.6 Hz, 1H and δ 7.75, d, J = 8.7 Hz, 1H; 6.81, d, J = 8.7 Hz, 1H for the two compounds, respectively). Moreover a singlet was present in the ^{1}H-NMR spectrum of these two compounds (δ 7.16, s, 1H) and δ 7.37, s, 1H). Apart from this the latter compound showed a signal indicative for a methoxy-group (δ 3.85, s,), which is absent in the former one. Due to the limited amount available, no additional NMR spectra could be recorded to obtain more structural information.

4. Conclusions

To indicate potentially multifunctional alkaloids present in *Psychotria nemorosa* leaves, chromatographic fingerprints were used in a chemometric approach to model the BChE and MAO-A inhibitory activities. In a first step, fingerprint data was aligned by Correlation Optimized Warping and analyzed by Principal Component Analysis. Then, by comparing the O-PLS1 regression coefficients with the fingerprints, four potentially multifunctional peaks were

507 indicated. Finally, a fraction containing the indicated compounds was assayed and exhibited a
508 very low IC_{50} for both enzymes, reinforcing the prediction from the O-PLS1 model. The above is
509 a very important strategy that was shown to be an improved alternative to old-fashion bioguided
510 fractionation and isolation of natural products. In this sense, time and costs can be saved and
511 the isolation of non-active or the reisolation of well-known compounds can be avoided, when
512 known compounds are identified from LC-MS analysis, for instance.
513 In the first part of this study [26], extraction and fraction methods were optimized based
514 on metabolite profiling. In the second part, the chromatographic profile was used for the
515 indication of peaks responsible for BChE and MAO-A inhibitory activity. Combining both parts,
516 this study demonstrates the importance of working with fingerprints for plant analysis. Because
517 of the complex nature of plant samples, their entire chemical composition must be taken into
518 account, affording good and accurate analytical approaches.
519

520 **Acknowledgements**

521 This work was supported by The National Council for Scientific and Technological
522 Development (CNPq), Fundação de Amparo à Pesquisa do Estado do Rio Grande do Sul
523 (FAPERGS), Brazil and by The Fund for Scientific Research (FWO), Vlaanderen, Belgium.
524 LCKJ, JS and ATH thank CNPq for the fellowships.
525

526 **References**

527 [1] A.L. Harvey, R. Edrada-Ebel, R.J. Quinn, The re-emergence of natural products for
528 drug discovery in the genomics era, Nat. Rev. 14 (2015) 111-129.
529 [2] C. Tistaert, B. Dejaegher, G. Chataigné, C. Rivière, N. Nguyen Hoai, M. Chau Van, J.
530 Quetin-Leclercq, Y. Vander Heyden, Potential antioxidant compounds in *Mallotus*

531 species fingerprints. Part II: fingerprint alignment, data analysis, and peak identification,
532 Anal. Chim. Acta 721 (2012) 35-43.
533 [3] C.J. Schulze, W.M. Bray, M.H. Woerhmann, J. Stuart, R. Scott Lokey, R. Linington,
534 "Function-first" lead discovery: mode of action profiling of natural product libraries using
535 image-based screening, Chem. Biol. 20 (2013) 285-295.
536 [4] U. Grienke, H. Braun, N. Seidel, J. Kirchmair, M. Richter, A. Krumbholz, S. von
537 Grafenstein, K.R. Liedl, M. Schmidtke, J.M. Rollinger, Compouter-guided approach to
538 access the anti-influenza activity of licorice constituents, J. Nat. Prod. 77 (2014) 563-
539 570.
540 [5] A.G. Atanasov, B. Waltenberger, E.-M. Pferschy-Wenzig, T. Linder, C. Wawrosch, P.
541 Uhrin, V. Temml, L. Wang, S. Schwaiger, E.H. Heiss, J.M. Rollinger, D. Schuster, J.M.
542 Breuss, V. Bochkov, M.D. Mihovilovic, B. Kopp, K. Bauer, V.M. Dirsch, H. Stuppner,
543 Discovery and resupply of pharmacologically active plant-derived natural products: a
544 review, Biotechnol. Adv. 33 (2015) 1582-1614.
545 [6] N. Nguyen Hoai, B. Dejaegher, C. Tistaert, V. Nguyen Thi Hong, C. Rivière, G.
546 Chataigné, K. Phan Van, M. Chau Van, J. Quetin-Leclercq, Y. Vander Heyden,
547 Development of HPLC fingerprints for *Mallotus* species extracts and evaluation of the
548 peaks responsible for their antioxidant activity, J. Pharm. Biomed. Anal. 50 (2009) 753-
549 763.
550 [7] C. Tistaert, B. Dejaegher, N. Nguyen Hoai, G. Chataigné, C. Rivière, V. Nguyen Thi
551 Hong, M. Chau Van, J. Quetin-Leclercq, Y. Vander Heyden, Potential antioxidant
552 compounds in *Mallotus* species fingerprints. Part I: indication, using linear multivariate
553 calibration techniques, Anal. Chim. Acta 649 (2009) 24-32.
554 [8] C. Tistaert, B. Dejaegher, G. Chataigné, C. Van Minh, J. Quetin-Leclercq, Y. Vander
555 Heyden, Dissimilar chromatographic systems to indicate and identify antioxidants from
556 *Mallotus* species, Talanta 83 (2011) 1198-1208.

557 [9] S. Thiangthum, B. Dejaegher, M. Goodarzi, C. Tistaert, A.Y. Gordien, N. Nguyen Hoai,
558 M. Chau Van, J. Quetin-Leclercq, Y. Vander Heyden, Potentially antioxidant
559 compounds indicated from *Mallotus* and *Phyllanthus* species fingerprints, J.
560 Chromatogr. B 910 (2012) 114-121.
561 [10] C. Tistaert, G. Chataigné, B. Dejaegher, C. Rivière, N. Nguyen Hoai, M. Chau Van, J.
562 Quetin-Leclercq, Y. Vander Heyden, Multivariate data analysis to evaluate the
563 fingerprint peaks responsible for the cytotoxic activity of *Mallotus* species, J.
564 Chromatogr. B 910 (2012) 103-113.
565 [11] A.T. Cardoso-Taketa, R. Pereda-Miranda, Y.H. Choi, R. Verpoorte, M.L.
566 Villarreal, Metabolic profiling of the Mexican anxiolytic and sedative plant *Galphimia*
567 *glauca* using nuclear magnetic resonance spectroscopy and multivariate data analysis,
568 Planta Med. 74 (2008) 1295-1301.
569 [12] M. Frédérich, Y.H. Choi, L. Angenot, F. Harnichfeger, A.W.M. Lefeber, R.
570 Verpoorte, Metabolomic analysis of *Strychnos nux-vomica*, *Strychnos icaja* and
571 *Strychnos ignatii* extracts by ^{1}H nuclear magnetic resonance spectrometry and
572 multivariate analysis techniques, Phytochemistry 65 (2004) 1993-2001.
573 [13] A.T. Henriques, R.P. Limberger, V.A. Kerber, P.R.H. Moreno, Alcaloides:
574 generalidades e aspectos básicos (Alkaloids: generalities and basic aspects), In:
575 C.M.O. Simões, E.P. Schenkel, G. Gosmann, J.C.P. De Mello, L.A. Mentz, P.R.
576 Petrovick, Farmacognosia: da planta ao medicamento (Pharmacognosy: from plant
577 until de medicine), Editora da UFRGS: Porto Alegre, 2007.
578 [14] P. Kittakoop, C. Mahidol, S. Ruchirawat, Alkaloids as important scaffolds in therapeutic
579 drugs for the treatments of cancer, tuberculosis, and smoking cessation, Curr. Top.
580 Med. Chem. 14 (2014) 239-252.

581 [15] E.L. Konrath, C.S. Passos, L.C. Klein-Júnior, A.T. Henriques, Alkaloids as a
582 source of potential anticholinesterase inhibitors for the treatment of Alzheimer's disease,
583 J. Pharm. Pharmacol. 65 (2013) 1701-1725.
584 [16] L.C. Klein-Júnior, C.S. Passos, A. Moraes, V. Wakui, E.L. Konrath, A. Nurisso,
585 P.-A. Carrupt, C.A.M. Oliveira, L. Kato, A.T. Henriques, Indole alkaloids and
586 semisynthetic indole derivatives as multifunctional scaffolds aiming the inhibition of
587 enzymes related to neurodegenerative diseases – a focus on *Psychotria* L. genus, Curr.
588 Top. Med. Chem. 14 (2014) 1056-1075.
589 [17] D.J. McKenna, G.H.N. Towers, F. Abbott, Monoamine oxidase inhibitors in South
590 American hallucinogenic plants: tryptamine and β-carboline constituents of Ayahuasca,
591 J. Ethnopharmacol. 10 (1984) 195-223.
592 [18] H. Achembach, M. Lottes, R. Waibel, G.A. Karikas, M.D. Correa, M.P. Gupta,
593 Alkaloids and other compounds from *Psychotria correae*, Phytochemistry 38 (1995)
594 1537-1545.
595 [19] C.S. Passos, T.C. Soldi, R.T. Abib, M.A. Apel, C. Simões-Pires, L. Marcourt, C.
596 Gottfried, A.T. Henriques, Monoamine oxidase inhibition by monoterpene indole
597 alkaloids and fractions obtained from *Psychotria suterella* and *Psychotria laciniata*, J.
598 Enzyme Inhib. Med. Chem. 28 (2013) 611-618.
599 [20] C.S. Passos, C.A. Simões-Pires, A. Nurisso, T.C. Soldi, L. Kato, C.M.A. Oliveira,
600 E.O. Faria, L. Marcourt, C. Gottfried, P.-A. Carrupt, A.T. Henriques, Indole alkaloids of
601 *Psychotria* as multifunctional cholinesterase and monoamine oxidases inhibitors,
602 Phytochemistry 86 (2013) 8-20.
603 [21] C.S. Passos, L.C. Klein-Júnior, J.M.M. Andrade, C. Matté, A.T. Henriques, The
604 catechol-*O*-methyltransferase inhibitory potential of *Z*-vallesiachotamine by *in silico* and
605 *in vitro* approaches, Braz. J. Pharmacog. 25 (2015) 382-386.

606 [22] L. Sacconnay, L. Ryckewaert, C.S. Passos, M.C. Guerra, L. Kato, C.M.A.
607 Oliveira, A.T. Henriques, P.-A. Carrupt, C. Simões-Pires, A. Nurisso, Alkaloids from
608 *Psychotria* target sirtuins: *in silico* and *in vitro* interaction studies, Planta Med. 81 (2015)
609 517-524.
610 [23] C.M. Taylor, Rubiacearum Americanarum Magna Hama XXXIII: The new group
611 *Palicourea* sect. *Didymocarpae* with four new species and two new subspecies
612 (Palicoureeae), Novon 23 (2015) 452-478.
613 [24] C.M. Taylor, Rubiacearum Americanarum Magna Hama XXXIV: The new group
614 *Palicourea* sect. *Tricephalium* with eight new species and a new subspecies
615 (Palicoureeae), Novon 24 (2015) 55-95.
616 [25] L.C. Klein-Júnior, C.S. Passos, J. Salton, F.G. Bitencourt, L.A. Funez, S.A.L.
617 Bordignon, A.L. Gasper, Y. Vander Heyden, A.T. Henriques, Evaluation of the
618 multifunctional monoamine oxidases and cholinesterases inhibitory effects of alkaloid
619 fractions obtained from species of the Palicoureeae Robbr. & Manen (or Psychotrieae
620 Cham. & Schltdl. s. lat.) tribe and their chemical profile by UPLC-MS analysis, Natural
621 Product Communications 11 (2016) (in press).
622 [26] L.C. Klein-Júnior, J. Viaene, J. Salton, M. Koetz, A.L. Gasper, A.T. Henriques, Y.
623 Vander Heyden, The use of chemometrics to study multifunctional indole alkaloids from
624 *Psychotria nemorosa* (*Palicourea comb. nov.*). Part I: extraction and fractionation
625 optimization based on metabolite profiling, DOI 10.1016/j.chroma.2016.07.030.
626 [27] N.-P.V. Nielsen, J.M. Carstensen, J. Smedsgaard, Aligning of single and multiple
627 wavelength chromatographic profiles for chemometric data analysis using correlation
628 optimised warping, J. Chromatogr. A 805 (1998) 17–35.
629 [28] B.G.M. Vandeginste, D.L. Massart, L.M.C. Buydens, S. de Jong, P.J. Lewi, J.
630 Smeyers-Verbeke, Handbook of Chemometrics and Qualimetrics. Part B, Elsevier,
631 Amsterdam, 1998.

[29] J.P.M. Andries, Y. Vander Heyden, L.M.C. Buydens, Predictive-property-ranked variable reduction with final complexity adapted models in partial least squares modeling for multiple responses, Anal. Chem. 85 (2013) 5444-5453.

[30] J. Trygg, S. Wold, Orthogonal projections to latent structures (O-PLS), J. Chemometr. 16 (2002) 119–128.

[31] G. Johson, S.W. Moore, Why has butyrylcholinesterase been retained? Structural and functional diversification in a duplicated gene, Neurochem. Int. 61 (2012) 783-797.

[32] F. Cerbai, M.G. Giovanini, C. Melani, A. Enz, G. Pepeu, N[1]phenethyl-norcymserine, a selective butyrylcholinesterase inhibitor, increases acetylcholine release in rat cerebral cortex: A comparison with donepezil and rivastigmine, Eur. J. Pharmacol. 572 (2007) 142–150.

[33] B. Li, J.A. Stribley, A. Ticu, W. Xie, L.M. Schopfer, P. Hammond, S. Brimijoin, S.H. Hinrichs, O. Lockridge, Abundant tissue butyrylcholinesterase and its possible function in the acetylcholinesterase knockout mouse, J. Neurochem. 75 (2000) 1320–1331.

[34] C.G. Ballard, N.H. Greig, A.L. Guillozer-Bongaarts, A. Enz, S. Darvesh, Cholinesterases: roles in the brain during health and disease, Curr. Alzheimer Res. 2 (2005) 307–318.

[35] K.K. O'Brien, B.K. Saxby, C.G. Ballard, J. Grace, F. Harrington, G.A. Ford, J.T. O'Brien, A.G. Swan, A.F. Fairbairn, K. Westes, T. del Sol, J.A. Edwardson, C.M. Morris, I.G. McKeith, Regulation of attention and response to therapy in dementia by butyrylcholinesterase, Pharmacogenetics 13 (2003) 231–239.

[36] M. Bortolato, K. Chen, J.C. Shih, Monoamine oxidase inactivation: from pathophysiology to therapeutics, Adv. Drug Deliver. Rev. 60 (2008) 1527-1533.

[37] M. Naoi, W. Maruyama, H. Yi, K. Inaba, Y. Akao, M. Shamoto-Nagai, Mitochondria in neurodegenerative disorders: regulation of the redox state and death

658 signaling leading to neuronal death and survival, J. Neural Transm. 116 (2009) 1371-
659 1381.
660 [38] M. Naoi, W. Maruyama, K. Inaba-Hasegawa, Y. Akao, Type A monoamine
661 oxidase regulates life and death of neurons in neurodegeneration and neuroprotection
662 Int. Rev. Neurobiol. 100 (2011) 85-106.
663 [39] M. Naoi, W. Maruyama, K. Inaba-Hasegawa, Type A and B monoamine oxidase
664 in age-related neurodegenerative disorders: their distinct roles in neuronal death and
665 survival, Curr. Top. Med. Chem. 12 (2012) 2177-2188.
666 [40] M.B.H. Youdim, J.J. Buccafusco, Multi-functional drugs for various CNS targets in
667 the treatment of neurodegenerative disorders, Trends Pharmacol. Sci. 26 (2005) 27-35.
668
669
670
671
672
673
674
675
676
677
678
679
680
681
682
683

684

685

686 **Figure captions**:

687

688 **Figure 1**. *Psychotria nemorosa* collection points.

689

690 **Figure 2.** Chromatographic fingerprints and correlation graphics (at the bottom) prior (a) and
691 after (b) warping. Experimental conditions: samples were analyzed by UPLC-DAD using an
692 Acquity BEH C_{18} UPLC column conditioned at 40 °C and eluted with a flow of 0.3 mL min^{-1} using
693 a mobile phase consisting of water (formic acid 0.1%) and methanol: 0 min (99 (A): 1 (B) v/v), 1
694 min (94:6), 4 min (94:6), 24 min (54:46), 25 min (54:46), 26 min (48:52), 28 min (48:52), 29 min
695 (0:100), 33 min (0:100), 35 min (99:1), 40 min (99:1). Detection was performed at 280 nm.

696

697 **Figure 3.** Chromatographic fingerprints (top figure) and the regression coefficients from PLS1
698 and O-PLS1 models butyrylcholinesterase inhibitory activity (a), and for monoamine oxidase-A
699 inhibitory activity (b).

700

701 **Figure 4.** The regression coefficients from PLS2 model for butyrylcholinesterase inhibitory
702 activity (BChE) (in blue) and for monoamine oxidase-A inhibitory activity (MAO-A) (in green).

703

704 **Figure 5.** Chromatographic fingerprints (experimental conditions see Figure 2) and the
705 regression coefficients from O-PLS1 models for butyrylcholinesterase inhibitory activity (BChE)
706 and for monoamine oxidase-A inhibitory activity (MAO-A). The arrows indicate potentially multi-
707 target compounds.

708

709 **Figure 6.** Chromatogram of the active fraction obtained by semi-prep HPLC. Experimental
710 conditions see Figure 2. Peaks 1-4 indicate multifunctional peaks.
711

Figure
Click here to download high resolution image

Figure
Click here to download high resolution image

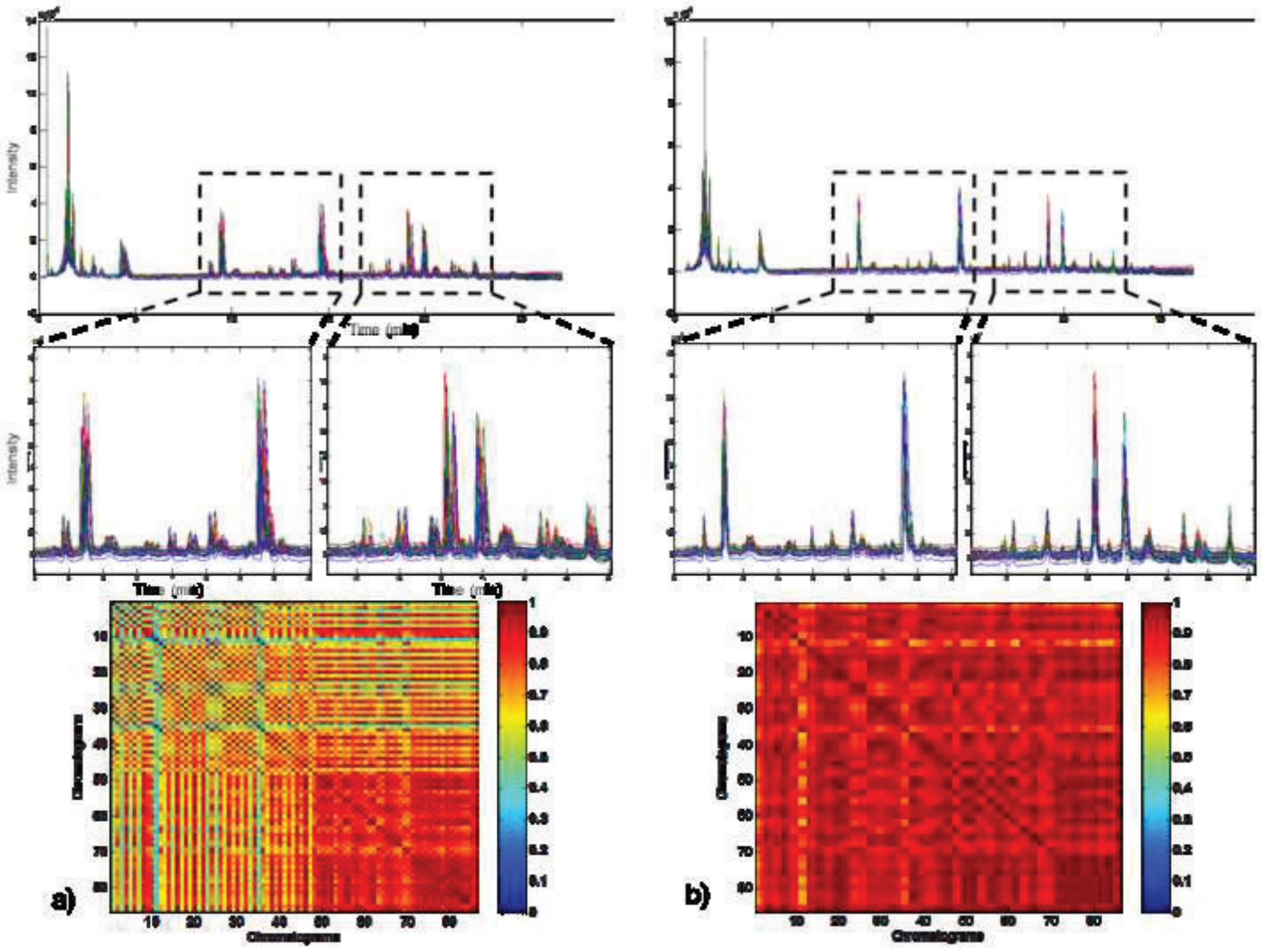

Figure
Click here to download high resolution image

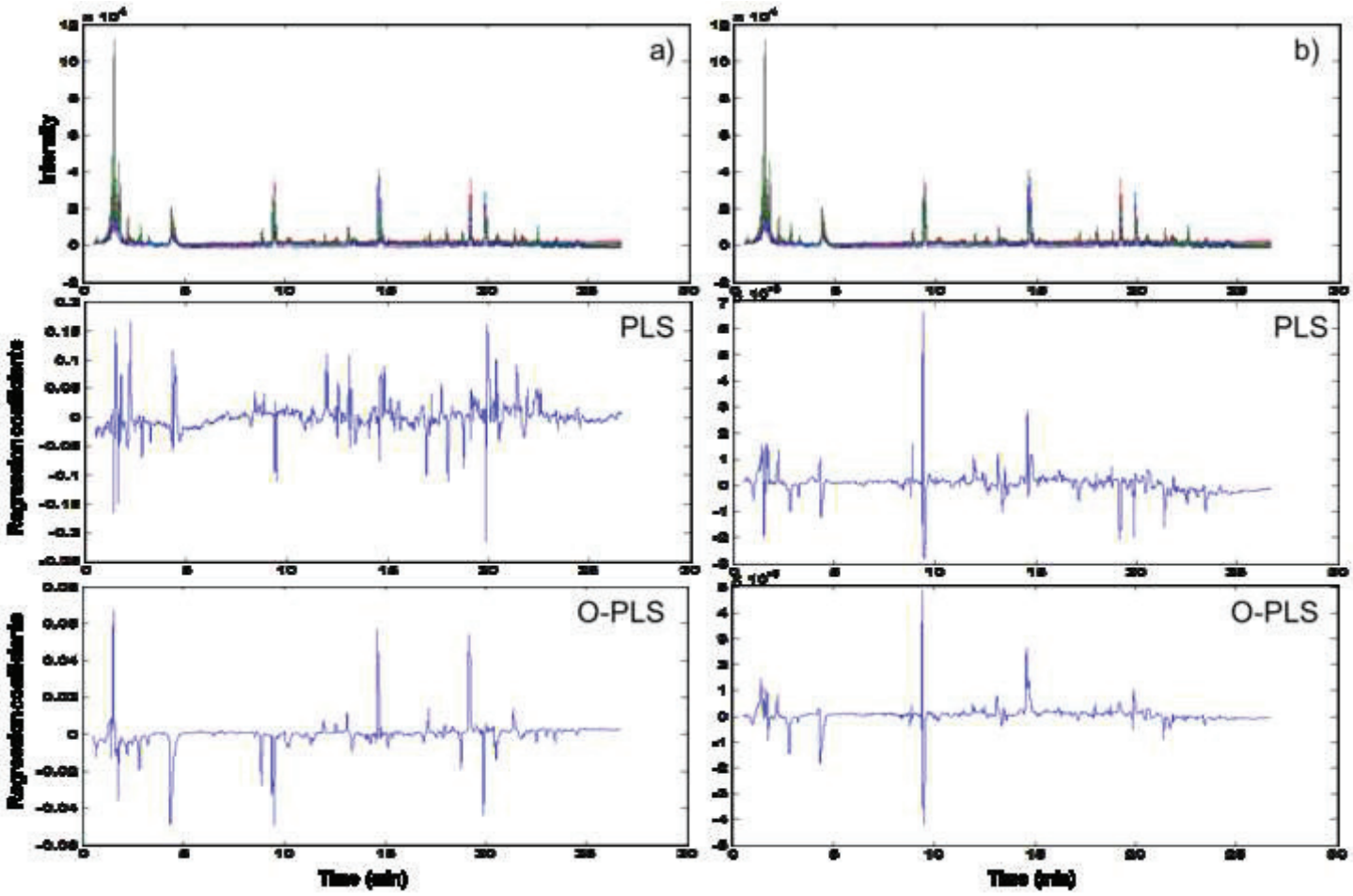

Figure
Click here to download high resolution image

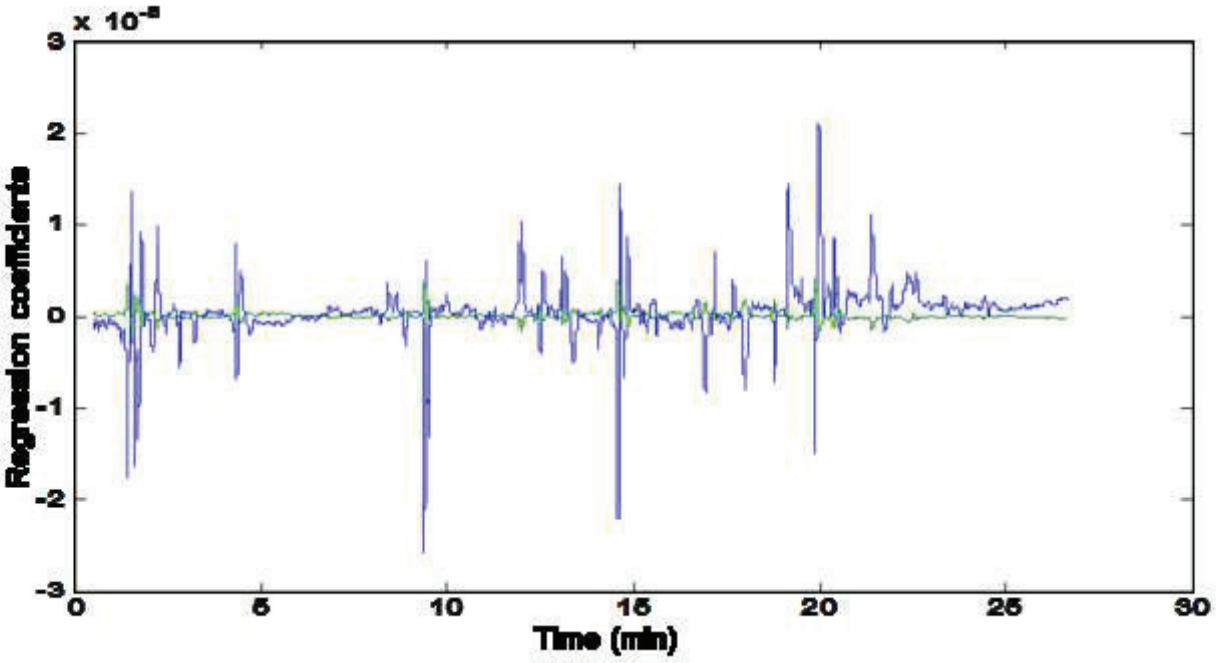

Figure
Click here to download high resolution image

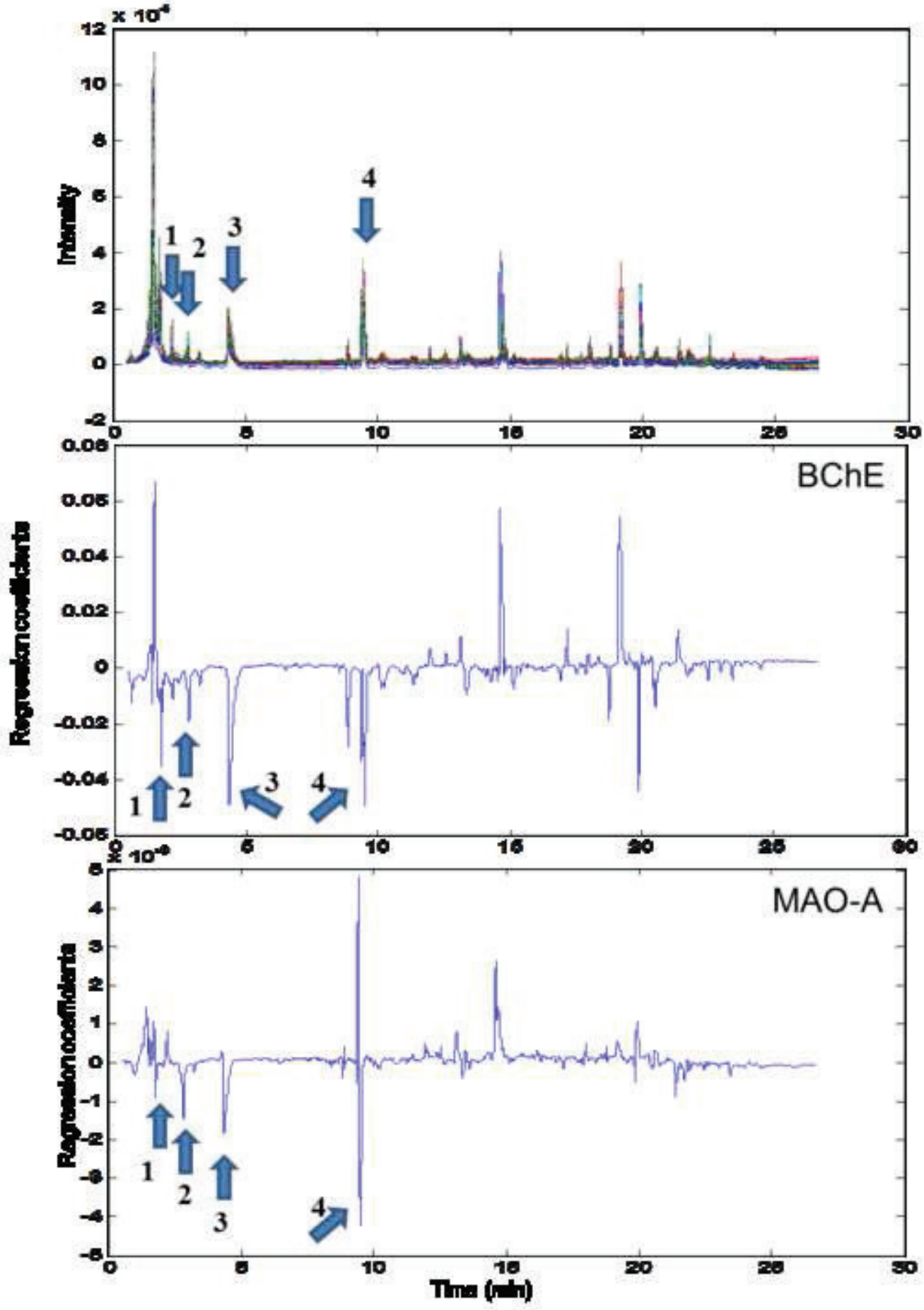

Figure
Click here to download high resolution image